Nanoscale

PAPER

View Article Online
View Journal | View Issue

Check for updates

Cite this: *Nanoscale*, 2020, **12**, 1495

Antenna-coupled vacuum channel nano-diode with high quantum efficiency

Shenghan Zhou,[a,b] Ke Chen,[a,b] Xiangdong Guo,[a,b] Matthew Thomas Cole,[a,b,c] Yu Wu,[d] Zhenjun Li,[a,b] Shunping Zhang,*[d] Chi Li*[a,b] and Qing Dai*[a,b]

Vacuum channel diodes have the potential to serve as a platform for converting free-space electromagnetic radiation into electronic signals within ultrafast timescales. However, the conversion efficiency is typically very low because conventional vacuum channel diode structures suffer from high surface barriers, especially when using lower energy photon excitation (near-infrared photons or lower). Here, we report on an optical antenna-coupled vacuum channel nano-diode, which demonstrates a greatly improved quantum efficiency up to ~4% at 800 nm excitation; an efficiency several orders of magnitude higher than any previously reported value. The nano diodes are formed at the cleaved edge of a metal–insulator–semiconductor (MIS) structure, where a gold thin film with nanohole array serves as both the metal electrode and light-harvesting antenna. At the nanoholes-insulator interface, the tunneling barrier is greatly reduced due to the coulombic repulsion induced high local electron density, such that the resonant plasmon induced hot electron population can readily inject into the vacuum channel. The presented vertical tertiary MIS junction enables a new class of high-efficiency, polarization-specific and wavelength- sensitive optical modulated photodetector that has the potential for developing a new generation of opto-electronic systems.

Received 18th July 2019,
Accepted 25th December 2019

DOI: 10.1039/c9nr06109f

rsc.li/nanoscale

Published on 26 December 2019. Downloaded by University of Bath on 2/9/2020 9:52:53 AM.

Introduction

Due to ballistic electron transport, vacuum devices support higher power operation, higher operational speeds and higher data transmission bandwidths than conventional solid-state electronic devices. For interelectrode gaps of less than 100 nm, integration challenges associated with the need for, and formation of ultra-high vacuum are removed, with effective transport through such gaps occurring even in air. With the emergence of ultra-precise nanoscale manufacturing, vacuum electronics are becoming increasingly feasible as a means of developing low-energy consumption, high-speed integrated opto-electronic devices.

Optical antennas can efficiently couple free-space light into nanoscale volumes. Such light-focusing properties are mediated by the formation of surface plasmons, a collective oscillation of free electrons with respect to the ion background. Integrating solid-state devices with metallic optical antenna has been widely employed in energy harvesting,[1–4] imaging,[5–7] and various light detection technologies.[8–10] Optical antennas have also been coupled into nanoscale vacuum devices,[11,12] which has the potential to mediate ultrafast light information processing. However, strong-field laser (around 10^{12} W cm^{-2} in the infrared range) is required to drive the electrons out of the high vacuum barrier (work function 4–5 eV), in the multiphoton and strong field regime.[11]

Here, we report on a highly-efficient optically modulated vacuum channel nano-diode array that operates in the relative weak light regime (<2×10^6 W cm^{-2}, in contrast to the above strong-field laser). A greatly enhanced quantum efficiency of ~4% is obtained at 800 nm excitation, achieved by exploiting a greatly reduced interfacial vacuum barrier at the edge of a metal–insulator–semiconductor (MIS) capacitor structure. Here, the nanoscale vacuum channel (length ~30 nm) is formed at the interface (thickness <10 nm) between cleaved insulator edge and air, which can support a ballistic transport of electrons. In the MIS capacitor structure, a quantum potential well is formed in the semiconductor side of the semiconductor–insulator interface. The quasi-two dimensional electron gas (2DEG)—an electron system that is confined in one spatial dimension but are free to move in two spatial dimensions, is formed due to the injection of electrons from

[a]*Division of Nanophotonics, CAS Center for Excellence in Nanoscience, National Center for Nanoscience and Technology, Beijing 100190, P. R. China. E-mail: lichi@nanoctr.cn, daiq@nanoctr.cn*
[b]*Center of Materials Science and Optoelectronics Engineering, University of Chinese Academy of Sciences, Beijing 100049, P. R. China*
[c]*Department of Electronic and Electrical Engineering, University of Bath, BA2 7AY, UK*
[d]*School of Physics and Technology, Wuhan University, Wuhan 430072, China. E-mail: spzhang@whu.edu.cn*

Published on 26 December 2019. Downloaded by University of Bath on 2/9/2020 9:52:53 AM.

doped semiconductor into the potential well.[13,14] At the edge of the 2DEG (formed at the cleaved edge of the nanohole structure), strong coulombic repulsion pushes the electrons towards to air side. Then, the electrons are accumulated at the edge of the 2DEG.[15,16] This will significantly change the electrostatic potential there, and thus reduce the effective vacuum barrier height.[17,18] The present research has significant potential in supporting the development of future ultrafast light information processing devices, such as plasmon enhanced photodetectors, and surface plasmon logic circuits.

Results and discussion

Device fabrication and operation principle

Fig. 1a schematically depicts the fabricated MIS structure. The vacuum channel nano-diodes were fabricated by spatially selective focused-ion-beam etching (FIB). The MIS structure consists of a 60 nm-thick Au layer, 30 nm-thick SiO_2 layer, on an n-type Si substrate (phosphorus-doped, 0.003 Ω cm, (100), 500 ± 10 μm). The active optical antenna coupled vacuum channel nano-diode consists of an array of independent, rectangular nanoholes etched into the n-Si substrate. Fig. 1b shows a scanning electron microscope (SEM) image of a representative fabricated device. A typical hole size is 500 (±12) nm × 100 (±18) nm. The distance between two adjacent holes is around 200 nm. Two perpendicular symmetry planes in the rectangular nanoholes support both longitudinal and transverse plasmon resonances, with the frequency of these resonances determined by the nanoholes' designed geometry.

In this diode structure, the channel length is determined by the controlled thickness of the insulator layer between the anode and the cathode. The insulator thickness (30 nm) was smaller than the mean free path of air (~69 nm) in order to allow for device in-air operation. Low-emission-barrier vacuum channel nano-diodes are formed at the edge the nanoholes, as shown in Fig. 1c. Fig. 1d shows the energy band diagram during negative bias. Compared with the inside (dotted line), the vacuum barrier is greatly reduced at the edge of the MIS structure (red line). Therefore, under laser irradiation on the top electrode, hot electrons are generated in the Au contact due to photon absorption. The generated hot electrons are excited to a higher energy level following their absorption of the incident photons energy. These energetic electrons thus more easily tunnel through the reduced barrier.

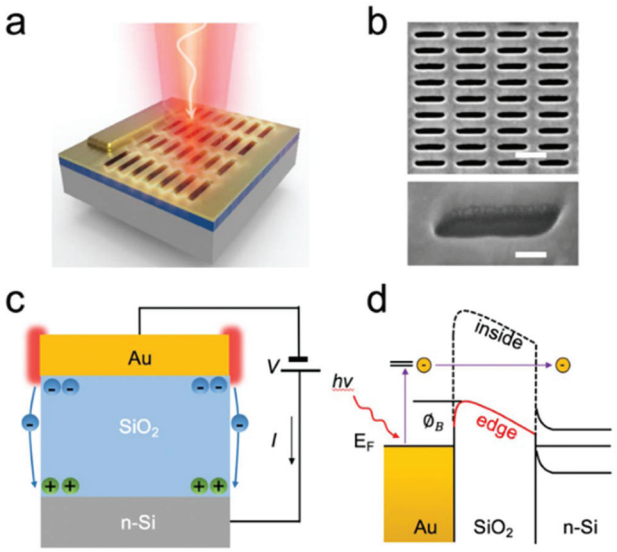

Fig. 1 The antenna coupled vacuum channel nanoscale diode. (a) Schematic depiction of the vacuum channel nano-diode fabricated by FIB etching consist of an array of rectangular nanoholes operating during laser induced plasmon resonance at the edge of MIS structure. (b) The top is scanning electron micrograph of a representative fabricated device (6 × 15 array with 500 nm × 100 nm, scale bar: 500 nm). The bottom is an edge of a nanohole at higher magnification (scale bar: 150 nm, tilt angle = 45°). (c) Schematic of the electron emission and transport in nano vacuum channels: Au electrode under negatively bias. Note the electron emission from the edge of 2DEG is from gold to silicon. (d) Energy band diagram with the Au electrode during negative bias. The dotted line indicates the energy band of the inside of MIS structure. Where ϕ_B is the barrier height, and E_f is Fermi level. During laser irradiation on the top electrode, electrons are excited to a higher energy level by gaining the energy of a photon and then tunneling through the barrier. The barrier height at the edge of MIS structure is greatly reduced than the inside.

Transport characteristics

The electrical properties of a representative set of 90 vacuum channel nano-diodes were measured (Keithley Model 4200-SCS). When applying a negative bias on the Au electrode with the Si grounded, the diodes revealed a typical negative biased characteristic; with electron emission in the Au-to-Si direction (Fig. 1c). The emission behavior of patterned and unpatterned MIS structures was explored. Fig. 2a shows typical static current-*versus*-voltage (*I*–*V*) curves of both patterned and unpatterned devices, in the dark, under different negative bias. A 300 pA (−1 V) leakage current (black line, Fig. 2a) was measured prior to FIB etching, which is significantly less than the tunneling current (60 nA at −1 V, red line, Fig. 2a) measured following device fabrication, suggesting morphological dependent enhancement in the emission current. In the absence of irradiation, the electrons in the nano-patterned one

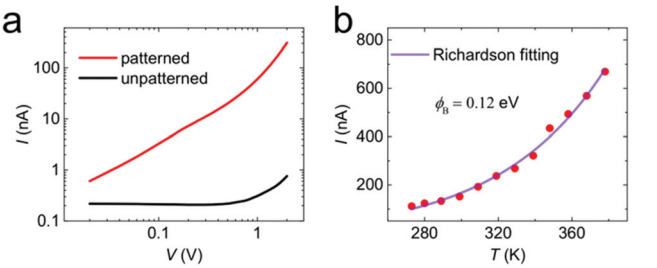

Fig. 2 Electron transport in the vacuum channel nanoscale diode. (a) Measured *I*–*V* characteristics of vacuum channel nano-diode under negatively bias. (b) The current curve of the representative device *versus* temperature (Au electrode biased to −2 V). The barrier height is 0.12 eV calculated by Richardson fitting.

This journal is © The Royal Society of Chemistry 2020

Published on 26 December 2019. Downloaded by University of Bath on 2/9/2020 9:52:53 AM.

can tunnel through the vacuum barrier easily than the flat Au, because the vacuum barrier is greater reduced at the edge of MIS structure.

The barrier height has also been explored through temperature-dependent transport studies. The local temperature changes the electron distribution of the local electron population. As the temperature increases a larger population of high-energy electrons results due to population thermalization. This excited electron population observe a vacuum barrier that is greatly reduced at the edge of the MIS structure, resulting in electron emission that is particularly temperature sensitive. The temperature-dependent electron emission properties of the representative devices was measured, as shown in Fig. 2b. According to thermionic emission theory, the height of vacuum barrier can be estimated by Richardson formula,

$$I = I_0\ (e^{qV/kT} - 1) \quad (1)$$

where I is the emission current, I_0 is the emission current at zero bias voltage, $I_0 = AKT^2e^{-q\phi_B/kT}$, V is the applied bias voltage, A is the device emission area, ϕ_B is the barrier height, T is the temperature, $K \approx 100$ A $(\mathrm{cm}^2\ \mathrm{K}^{-2})^{-1}$ is Richardson constant and the k is Boltzmann constant. When the top electrode is negatively biased (−2 V), the vacuum barrier height at the edge of the MIS structure is of the order of ~0.12 eV, which is much lower than 0.5 eV (ref. 10) and 2.6 eV (ref. 19) previous reported for similar devices.

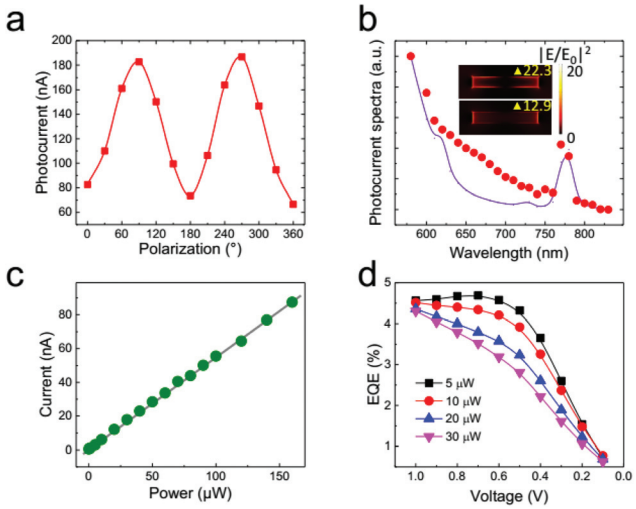

Fig. 3 Photo response characteristics of the vacuum channel nanoscale diode. (a) Photocurrent polarization dependence during device excitation at λ = 633 nm. Angle 0° of polarization is parallel to the long axis. (b) Theoretically calculated absorption spectra (purple line) and experimentally measured photocurrent spectra (red points) of the device at polarizer angle 0° (parallel to the long axis). Inset: electromagnetic field distribution of the device extracted from the purple line in Fig. 3b. The maximum of $|E/E_0|^2$ is 22.3 and 12.9 at λ = 780 nm (top) and λ = 710 nm (bottom), respectively. (c) Photocurrent for the representative device as a function of input laser power (Au electrode biased to −1 V). (d) Plot of the measured external quantum efficiency (EQE) as a function of applied voltage for different input laser power.

Photo response

Having demonstrated the occurrence of low-barrier electron emission at the MIS edges, we now investigate the photo response of the device. We aim to realize an enhanced photo response on the patterned MIS structure; in so far as demonstrating that the energetic electrons excited by the plasmon resonance can transport by readily tunneling through the greatly reduced vacuum barrier.

90 vacuum channel nano-diodes were tested under illumination (λ = 800 ± 6 nm) from a picosecond (τ = 100 ps) ultrafast laser (Wuhan YSL Photonics, SC-Pro7). This optical excitation was focused on the sample using a 10× microscope objective to produce a 10 μm diameter spot size. Here we demonstrate that the photocurrent generation results from hot electron emission and that such emission can be dramatically enhanced by driving a surface plasmon resonance in the Au electrode. Initially hot electrons are generated in the Au contact due to photon absorption. The generated hot electrons are readily injected into the oxide due to the reduced barrier. The injected electrons cross the oxide and contribute to the measured photocurrent.

Fig. 3 shows the photo response characteristics of the vacuum channel nano-diodes. The photocurrent obtained from our devices is determined directly by the geometric properties of the etched nanohole-based antenna. The polarization dependence of the photocurrent also follows that of the geometrically asymmetric nanoholes which provide a highly polarization dependent response (Fig. 3a).[20,21] For light polarized along the long (transverse) axis, we observe >50% attenuation of the photocurrent with respect to the longitudinal polarization.

The spectral response directly follows the transverse dipole absorption resonance of the plasmon mode excited on the structure. Responsivity curves of the device are shown in Fig. 3b. Significant agreement between experimental photocurrent spectra (red points, Fig. 3b) as a function of antenna resonant frequency and optical absorption spectra calculated using theoretical methods (purple line, Fig. 3b) is noted. As shown in Fig. 3b, when the laser polarization is 0° (parallel to the long axis), the measured photocurrent spectrum has a peak near 780 nm, consistent with the peak position of the simulated plasmon resonance. The inset of Fig. 3b shows the simulated electromagnetic field distribution of the device extracted from the purple line in Fig. 3b at λ = 780 nm (top) and λ = 710 nm (bottom), respectively. The plasmon resonance intensity at 780 nm ($|E/E_0|^2_{max}$ = 22.3) is significantly stronger than at 710 nm ($|E/E_0|^2_{max}$ = 12.9), corresponding to the photocurrent spectrum in Fig. 3b. When photocurrent measurements are performed on multiple antenna arrays, each with a different resonant frequency, it is envisaged that such devices may function as a nanoscale single-chip spectrometer. This spectroscopic functionality is due to the relationship between photocurrent amplitude and the amplitude of the plasmon resonance at a given frequency and this spectral

Published on 26 December 2019. Downloaded by University of Bath on 2/9/2020 9:52:53 AM.

sensitivity can be used to determine the wavelength of the incident light.

The change in illumination optical power at a single wavelength (λ = 800 nm) results in a linear response with photocurrent. The photocurrent is developed from a single incident photon to a single hot electron within this range of incident light intensities.[22–26] The corresponding *I–P* curve is shown in Fig. 3c. Significant linearity is noted, which supports our claim of linearity in the photocurrent generation process with absorbed light power.

The overall quantum efficiency of the vacuum channel nano-diodes depends critically on the characteristics of their constituent materials (principally the metal work function and semiconductor Femi level) as well as the specifics of the device geometry. There is a significant interplay in how these factors affect the generation of hot electrons, and the probability for the contribution of the generated hot electrons to the photocurrent. For instance, Park *et al*. demonstrated that the internal photoemission efficiency of metal–insulator–metal (MIM) or metal–semiconductor (MS) nano-diodes is influenced simultaneously by the thickness and morphology of the metal layer.[27,28] We may define external quantum efficiency (EQE) as the ratio of the number of hot electrons emitted tunneling through the barrier divided by the number of photons incident on the nanohole, as:

$$\mathrm{EQE} = \frac{hc}{e\lambda} R(\lambda) \quad (2)$$

where h is Planck constant, c is the velocity of light in vacuum, e is the electron charge and λ is the wavelength of the incident laser. The spectral responsivity, $R(\lambda) = \Delta I/P_{\mathrm{optical}}$, is the ratio of the response current to the incident monochromatic optical power (the responsive photocurrent and the laser power incident on the device are denoted by ΔI and P_{optical}, respectively). Table 1 compares the present study with other reported similar structures. All previously reported high EQE values to date have been obtained at shorter wavelengths. Here, based on our empirical findings, we calculate an EQE of ~4% at different laser powers (Fig. 3d), which was achieved at long wavelength (λ = 800 nm), resulting in an EQE several orders of magnitude higher than other similar devices.

Conclusions

Here we have demonstrated photoelectron generation by hot electron formation in a new vacuum channel nano-diodes structure. The voltage-dependence, temperature-dependence, laser power-dependence, polarization-dependence and spectra-dependence of the photocurrent have all been experimentally determined. The EQE of the vacuum channel nano-diodes was ~4%, several orders of magnitude higher than other similar devices. Moreover, the absorption peak of the photo-response current have been corroborated by theoretical calculations and experimental verification. By utilizing arrays of nano-diodes as direct light collection and carrier generation elements, both polarization and wavelength selective detectors can be implemented without the need for additional costly, bulky and fragile optical components. The investigated device has shown impressive functionality as a high-efficiency light modulation detector in weak light environments. With a diverse range of potential applications, the present nano MIS structures offer a new method of mediating light–matter interactions, creating additional and unpredictable applications in the fields of light-sensing, energy conversion and miniaturized photodetection technologies.

Experimental section

Fabrication process of vacuum channel nanoscale diode

The vacuum channel nano-diodes were fabricated by performing FIB etching on a silicon MIS substrate. A 30 nm-thick SiO_2 layer was first grown by atomic layer deposition (ALD, SI-ALD) on n-type silicon (phosphorus-doped, resistivity = 0.003 Ω cm) wafers ((100)-oriented; thickness, 500 ± 10 μm). A gold electrode (thickness, 60 nm) was prepared on the top of the insulator layer by electron beam evaporation in conjunction with an electron beam lithography and lift-off process. After the formation of the MIS structure, the MIS wafers were further processed to develop nanoscale-void vertical channels using a FIB etching technique. The FIB etching process was performed with a FIB/SEM Dual Beam System (FEI-Nova200). A gallium ion beam (30 keV, 10 pA) was used with a dwell time of 39 s to create rectangular nanoholes arrays (cross-sections, 500 nm × 100 nm) in silicon MIS wafers (Fig. 1b).

Table 1 Comparison of typical plasmonic hot electron nanoscale diode performance parameters

Structure	Materials	Excitation wavelength	EQE	Ref.
MS structure	Ag/Au–TiO_2	380 nm	2% (IQE)	27
MIM structure	Au–TiO_2–Ti	450 nm	12% (IQE)	28
MIS structure	FTO–TiO_2–Al_2O_3–Ag	460 nm	4%	29
MIS structure	FTO–TiO_2–Al_2O_3–Au	550 nm	1.3%	29
MIM structure	Ag–polymer–Ag	680 nm	0.18%	30
MIS structure	Au–SiO_2–Si	720 nm	0.01% (IQE)	31
Lateral tunnel junction	Au	730–780 nm	0.03%	32
MIS structure	Au–SiO_2–Si	800 nm	4%	Our work
Nanowire array	Au/Ti–SiO_2	1200–1800 nm	0.05–0.1% (IQE)	33
Nanorods array	ITO–SiO_2–Au	1250–1600 nm	0.01% (IQE)	10
Nano grating structure	Au–Si	1295–1635 nm	0.2% (IQE)	34

This journal is © The Royal Society of Chemistry 2020

Published on 26 December 2019. Downloaded by University of Bath on 2/9/2020 9:52:53 AM.

Characterization and electronic measurements

The morphologies of the vacuum channel nano-diodes were characterized by SEM (FEI NOVA Nano-430). The *I–V* characteristics of the vacuum channel nano-diodes were measured in the dark with a semiconductor parameter analyzer (Keithley Model 4200-SCS). Incident light from a supercontinuum laser source (Wuhan YSL Photonics, SC-Pro7) was focused on the sample using 10× Olympus objective (MplanFL, NA = 0.50) and the photoresponse was measured using a Keithley sourcemeter 2636B. The optical images were obtained by the same objective, and recorded using a CCD camera (DVC company, 710M-00-FW) to confirm the laser position on the nanoholes.

Simulations

Optical absorption spectra and electromagnetic field distributions were simulated using the finite element method.

Conflicts of interest

There are no conflicts to declare.

Acknowledgements

This work was supported by the National Key R&D Program of China (Grant No. 2016YFA0202001), the National Natural Science Foundation of China (Grant No. 11427808, 51972072 and 51602071), the Key Research Program of the Chinese Academy of Sciences (grant no. ZDBS-SSW-JSC002), CAS Interdisciplinary Innovation Team (grant no. JCTD-2018-03), and the Strategic Priority Research Program of the Chinese Academy of Sciences (grant no. XDB50020200 and XDPB06).

References

1 S. Obayya, N. F. F. Areed, M. F. O. Hameed and M. H. Abdelrazik, *Optical nano-antennas for energy harvesting*, IGI Global, 2015.
2 E. Briones, J. Alda and F. Javier Gonzalez, *Opt. Express*, 2013, **21**, A412–A418.
3 G. A. E. Vandenbosch and Z. Ma, *Nano Energy*, 2012, **1**, 494–502.
4 M. Dagenais, K. Choi, F. Yesilkoy, A. N. Chryssis and M. C. Peckerar, in *Optoelectronic Integrated Circuits Xii*, ed. L. A. Eldada and E. H. Lee, 2010, vol. 7605.
5 R. L. Olmon, P. M. Krenz, A. C. Jones, G. D. Boreman and M. B. Raschke, *Opt. Express*, 2008, **16**, 20295–20305.
6 C. Hoppener and L. Novotny, *Nano Lett.*, 2008, **8**, 642–646.
7 A. Weber-Bargioni, A. Schwartzberg, M. Cornaglia, A. Ismach, J. J. Urban, Y. Pang, R. Gordon, J. Bokor, M. B. Salmeron, D. F. Ogletree, P. Ashby, S. Cabrini and P. J. Schuck, *Nano Lett.*, 2011, **11**, 1201–1207.
8 W. Li, Z. J. Coppens, L. V. Besteiro, W. Wang, A. O. Govorov and J. Valentine, *Nat. Commun.*, 2015, **6**, 8379.
9 L. Novotny and N. van Hulst, *Nat. Photonics*, 2011, **5**, 83–90.
10 M. W. Knight, H. Sobhani, P. Nordlander and N. J. Halas, *Science*, 2011, **332**, 702–704.
11 W. P. Putnam, R. G. Hobbs, P. D. Keathley, K. K. Berggren and F. X. Kaertner, *Nat. Phys.*, 2017, **13**, 335–339.
12 T. Rybka, M. Ludwig, M. F. Schmalz, V. Knittel, D. Brida and A. Leitenstorfer, *Nat. Photonics*, 2016, **10**, 667–670.
13 T. Ando, A. B. Fowler and F. Stern, *Rev. Mod. Phys.*, 1982, **54**, 437–672.
14 A. Toriumi, M. Yoshimi, M. Iwase, K. Taniguchi and C. Hamaguchi, *Surf. Sci.*, 1986, **170**, 363–369.
15 S. Han and J. Ihm, *Phys. Rev. B: Condens. Matter Mater. Phys.*, 2000, **61**, 9986–9989.
16 X. Zheng, G. Chen, Z. Li, S. Deng and N. Xu, *Phys. Rev. Lett.*, 2004, **92**, 106803.
17 A. Mayer, *Phys. Rev. B: Condens. Matter Mater. Phys.*, 2005, **71**, 235333.
18 S. Srisonphan, Y. S. Jung and H. K. Kim, *Nat. Nanotechnol.*, 2012, **7**, 504–508.
19 H. Chalabi, D. Schoen and M. L. Brongersma, *Nano Lett.*, 2014, **14**, 1374–1380.
20 R. Dhama, V. Caligiuri, L. Petti, A. R. Rashed, M. Rippa, R. Lento, R. Termine, H. Caglayan and A. Luca, *ACS Nano*, 2018, **12**, 504–512.
21 J. H. Zhang, M. ElKabbash, R. Wei, S. C. Singh, B. Lam and C. L. Guo, *Light: Sci. Appl.*, 2019, **8**, 13.
22 J. Hofmann and W. Steinman, *Phys. Status Solidi*, 1968, **30**, K53–K56.
23 J. G. Endriz and W. E. Spicer, *Phys. Rev. Lett.*, 1970, **24**, 64–68.
24 T. Inagaki, K. Kagami and E. T. Arakawa, *Phys. Rev. B: Condens. Matter Mater. Phys.*, 1981, **24**, 3644–3646.
25 T. Inagaki, K. Kagami and E. T. Arakawa, *Appl. Opt.*, 1982, **21**, 949–954.
26 J. Lehmann, M. Merschdorf, W. Pfeiffer, A. Thon, S. Voll and G. Gerber, *Phys. Rev. Lett.*, 2000, **85**, 2921–2924.
27 H. Lee, Y. K. Lee, E. Hwang and J. Y. Park, *J. Phys. Chem. C*, 2014, **118**, 5650–5656.
28 C. Lee, I. I. Nedrygailov, Y. K. Lee, C. Ahn, H. Lee, S. Jeon and J. Y. Park, *Nanotechnology*, 2015, **26**, 445201.
29 F. P. G. de Arquer, A. Mihi, D. Kufer and G. Konstantatos, *ACS Nano*, 2013, **7**, 3581–3588.
30 H. Qian, S.-W. Hsu, K. Gurunatha, C. T. Riley, J. Zhao, D. Lu, A. R. Tao and Z. Liu, *Nat. Photonics*, 2018, **12**, 485–488.
31 H. Goktas, F. S. Gokhan and V. J. Sorger, *ACS Photonics*, 2018, **5**, 4928–4936.
32 J. Kern, R. Kullock, J. Prangsma, M. Emmerling, M. Kamp and B. Hecht, *Nat. Photonics*, 2015, **9**, 582–586.
33 M. W. Knight, Y. Wang, A. S. Urban, A. Sobhani, B. Y. Zheng, P. Nordlander and N. J. Halas, *Nano Lett.*, 2013, **13**, 1687–1692.
34 A. Sobhani, M. W. Knight, Y. Wang, B. Zheng, N. S. King, L. V. Brown, Z. Fang, P. Nordlander and N. J. Halas, *Nat. Commun.*, 2013, **4**, 1643.